Journal of Thermal Analysis, Vol. 49 (1997) 525-533

THERMAL ANALYSIS STUDY OF THE EFFECT OF MOLECULAR WEIGHT ON CONSTRAINED AMORPHOUS PHASE IN POLY(PHENYLENE SULFIDE)

Sharon Xin Lu and Peggy Cebe***

Department of Physics and Astronomy, Tufts University, Science and Technology Center, Medford, MA 02155, USA

Abstract

We report a thermal analysis study of the effect of molecular weight on the amorphous phase structure of poly(phenylene sulfide), PPS, crystallized at temperatures just above the glass transition temperature. Thermal properties of Fortron PPS, having viscosity average molecular weights of 30000 to 91000, were characterized using temperature modulated differential scanning calorimetry (MDSC). We find that while crystallinity varies little with molecular weight, the heat capacity increment at the glass transition decreases as molecular weight decreases. This leads to a smaller liquid-like amorphous phase, and a larger rigid amorphous fraction, in the lower molecular weight PPS. For all molecular weights, constrained fraction decreases as the scan rate decreases.

Keywords: constrained amorphous phase, modulated differential scanning calorimetry, molecular weight, poly(phenylene sulfide)

Introduction

Poly(phenylene sulfide) is a semicrystalline polymer with a glass transition temperature at about 90°C, and a melting temperature (T_m) of 280°C from differential scanning calorimetry (DSC) [1–4]. Its structure and properties can vary quite significantly with previous thermal history [1–6] and with molecular weight [7, 8]. Several research groups have studied the effect of molecular weight on the crystallization kinetics of PPS [4, 7–12]. It is found that the crystallization rate of PPS decreases as molecular weight increases [7, 9]. Asymmetric linear growth rate curves are seen for PPS [4, 13]. Non-isothermal crystallization was studied by Collins *et al.* [10, 11].

In this work, we examine the effects of molecular weight on the structure of the amorphous phase in semicrystalline PPS. In this polymer, the amorphous phase has been shown to be highly constrained by the crystals, leading to a reduction in its

* Present address: Johnson and Johnson, Sommerville, New Jersey.

**Author to whom all correspondence should be addressed.

0368–4466/97/ $ 5.00

John Wiley & Sons Limited
Chichester

molecular mobility [2, 5, 6]. The quantification of the effect of chain constraint is done through thermal analysis of the heat capacity increment, $\Delta C_p(T)$, at the glass transition [2, 5, 6]. Although many reports exist on the effects of molecular weight on crystallization kinetics [7–12], so far there have been no studies of the effects of molecular weight on the structure of the amorphous phase and the constraining effects of crystals. It was our hypothesis that lower molecular weight polymer would have more taut tie molecules between crystals, leading to larger rigid amorphous fraction. Here we report effects of molecular weight on structure of PPS crystallized close to T_g. A more extensive study including results of small angle X-ray scattering and dynamic mechanical behavior will be reported later [14].

Since the rate of formation of crystals will likely be an important factor in creating constraints on the amorphous phase, we decided to minimize this effect among the different molecular weight samples by selecting different isothermal crystallization temperatures that would guarantee identical rates of crystallization. With kinetic rate effects minimized, the influence of molecular weight on structure could more easily be assessed. Small angle X-ray scattering studies [14] confirm that the crystallization kinetics are the same for all materials crystallized so as to have the same half-time. SAXS also reveals [14] that the long period varies with molecular weight, while the lamellar thickness does not vary (within experimental error). Thus, to the best of our ability we have kept the structure of the materials roughly the same by choosing crystallization conditions of constant half-time for the different samples.

We characterize the relative phase fractions in our PPS materials using DSC and MDSC [15–19]. MDSC is able to separate the total heat flow (T) into two parts. One is the result of the heat capacity effect, such as glass transition and melting, often referred to as reversing heat flow (R), and is the sample response in phase with the sinusoidal temperature profile. The difference between T and R is used to obtain a third heat flow, the result of the non-heat capacity effect, such as cold crystallization, often referred to as non-reversing heat flow (NR) [17].

Experimental section

Different molecular weight powders of Fortron™ PPS, were obtained from Hoechst Celanese and are referred to as F-200, F-214 and F-300. The viscosity average molecular weight (M_v) are listed in Table 1 and range from 30000 to 91000. Amorphous films were prepared by melting the powder in a hydraulic hot press between two pieces of Kapton™ film at 320°C for 2 min to destroy the crystallization seed nuclei, then quickly quenching into ice water. The amorphous samples obtained were transparent and showed no birefringence upon rotation under crossed polarizers. Some of these amorphous samples were used directly in our study. Others were crystallized at cold crystallization temperatures T_c (from 110.6 to 135°C).

A TA Instruments 2920 DSC was used for thermal property measurements. MDSC scanning rates were 5 and 3.5°C min^{-1}. The modulation amplitude and period were varied according to the manufacturer's recommendation [17] to ensure

Table 1 Viscosity average molecular weight, glass transition temperature and non-isothermal cold crystallization temperature of amorphous samples, and isothermal cold crystallization temperature of Fortron PPS

Fortron PPS	M_v[a]	T_g[b] / °C	$T_{c,nI}$[c] / °C	T_c[d] / °C
F-200	30000	84	112	110.6
F-214	50000	90	116	116.0
F-300	91000	92	133	135.0

[a] From viscosity determined in 1-chloronaphthalene at 208°C
[b] Glass transition of quenched amorphous sample scanned at 3.5°C min^{-1}
[c] Peak of the crystallization exotherm in amorphous samples, scanned at 3.5°C min^{-1}
[d] Isothermal cold crystallization temperatures chosen for a crystallization half-time of 200 s.

that almost no cooling occurred during the experiments. Sample mass was between 5 and 7 mg and experiments were performed under a nitrogen gas flow of 30 ml min^{-1}. The empty reference pan was matched in mass to the sample pan to within 0.05 mg. Indium was used to calibrate temperature and heat flow throughout the MDSC study.

The heat of fusion of perfect PPS crystals was taken to be 112 J g^{-1} [5]. Sapphire was used to calibrate the heat capacity. Heating rate of 20°C min^{-1} was used in the non-modulated mode (similar to ordinary DSC).

Wide angle X-ray scattering was performed using a rotating anode Rigaku RU300 generator operating at 45 kV and 60 mA with diffracted beam monochromator. Samples were examined in $\Theta/2\Theta$ reflection mode with $\lambda=1.54$Å. Calibration of peak position was made using National Institute of Standards and Technology silicon powder standard.

Results and discussion

Figure 1 shows the total heat flow curves *vs.* temperature for quenched amorphous F-200 (dashes) and F-300 (solid line), respectively. The scan rate is 3.5°C min^{-1}, and these scans were taken only up to 175°C. The total heat flow curves show the same information as is provided by non-modulated DSC. The glass transition relaxation is followed by a sharp crystallization exotherm. T_g and T_c data are listed in Table 1. Comparing F-200 with F-300, we see that the position of the crystallization exotherm in F-300 is about 20 degrees above that of F-200. The crystallization kinetics of F-300 are much slower than F-200 due to the factor of three difference in molecular weight. For this reason, selecting the same crystallization temperatures for both materials would not provide comparable crystal structures. We used detailed crystallization studies of these two materials [14] to select cold crystallization temperatures that would yield the same rate of crystallization, i.e., the same half-time for crystallization. To provide a half-time of 200s, F-200 is crystallized at 110.6°C, F-214 is crystallized at 116°C, and F-300 is crystallized at 135°C. The isothermal cold crystallization temperatures are listed in the last column of Table 1.

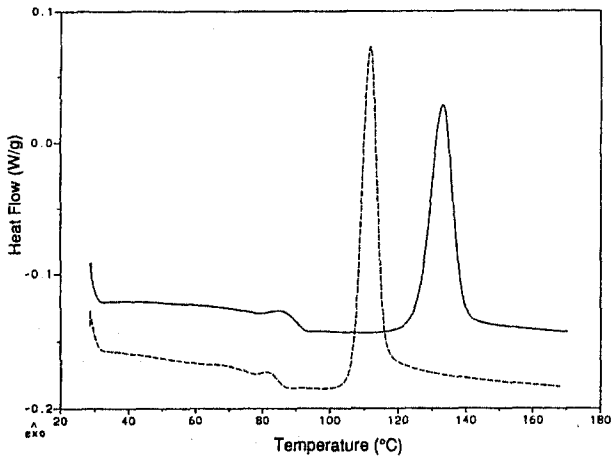

Fig. 1 MDSC total (*T*) heat flow *vs.* temperature for quenched amorphous Fortron™ PPS. Scan rate was 5 °C min^{-1}, with oscillation amplitude of 0.796 °C and period of 60 s. F-200 (dashed line); F-300 (solid line)

Figure 2 shows MDSC raw data, modulated heat flow curve (upper curve) and derivative of the modulated temperature, or heating rate (lower curve), for F-200 crystallized at 110.6 °C to give a half-time of 200 s. This material was scanned through the melting region at an average heating rate of 5 °C min^{-1}, with an oscillation amplitude of ± 0.796 °C every 60 s. The heating rate curve is above zero during most of the scan, indicating that the sample is nearly always heated and not cooled. Only during the first order melting phase transition does the heating rate go momentarily below zero, owing to the difficulty in oscillating the temperature of the

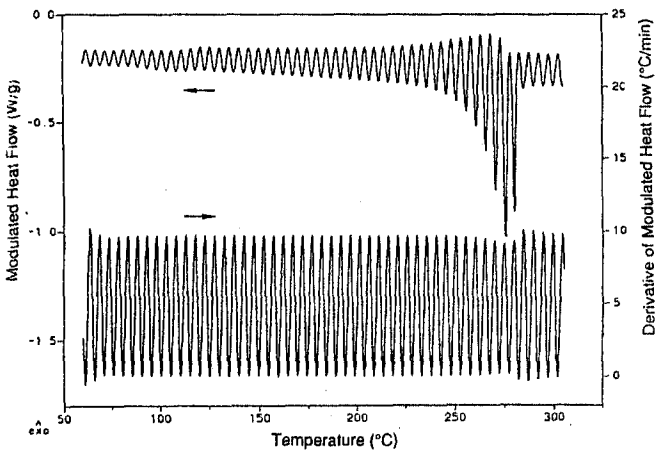

Fig. 2 MDSC raw data for Fortron™ F-300 PPS cold crystallized at 110.6 °C with $t_{1/2}$ = 200 s. Scan rate was 5 °C min^{-1}, with oscillation amplitude of 0.796 °C and period of 60 s. Modulated heat flow (left hand axis) and simultaneous derivative of the modulated temperature, or heating rate, (right hand axis) *vs.* scanning temperature

entire sample, when a portion of it is remaining at constant temperature during its phase transition.

The raw data are used to derive the total (T), reversing (R), and non-reversing (NR) heat flow signals for F-200. Similarly, raw data were acquired for F-214 and F-300 crystallized with the same half-time of 200s but these raw data are not shown for the sake of brevity. To facilitate comparison among the molecular weights, the T curves are all plotted together in Fig. 3a, the R curves in Fig. 3b, and the NR curves in Fig. 3c.

In Fig. 3a, for F-200 crystallized at 110.6°C, the T curve shows an exothermic step at about 115°C followed by the major melting endotherm at 284°C. For F-214, the T curve shows the same features as F-200, with different temperatures. The exothermic step begins at 120°C, just after the glass transition. There follows an endotherm at 282.5°C. For F-300, the T curve shows the initiation of crystallization at about 145°C, followed by melting at 277°C. All three curves become flat when the temperature is above 285°C, indicating that all the crystals have melted. All three materials have about the same net area ΔH^T, ($\Delta H^T = A_{endo} - A_{exo}$) under the total heat flow curves, indicating that the initial level of crystallinity is about the same, in spite of the differences in their crystallization temperatures. This result is supported by both wide and small-angle X-ray scattering studies to be reported separately [14]. The main difference among the T curves is the initiation point for the further crystallization of the sample, which occurs just above the prior treatment temperature of each sample. Arrows mark the treatment temperatures for these samples.

Figure 3b shows the R curves for the three molecular weights. For F-200, the R curve shows the glass transition relaxation at 101°C, and the melting endotherm at 283°C. F-214 R curve shows the glass transition at 103°C, and the melting endotherm at 282°C. Finally, in the R curve of F-300, the glass transition relaxation occurs at 102°C and the melting endotherm at 277°C. The major difference occurs in the glass transition region and the steady decrease in the area under the R curve, as the molecular weight increases. ΔH^R follows the rank ordering: F-200 > F-214 > F-300. F-200 forms the largest amount of crystals during the scan – F-300 forms the least.

The NR curves, shown in Fig. 3c, have only exothermic features. In F-200, crystallization starts at about 114°C, which is just above the previous cold crystallization temperature, and continues to a large exothermic peak at 280°C. F-214 shows a crystallization exotherm starting with an upturn at about 120°C, and a large peak at 278°C. Finally, F-300 NR curve has an upturn at about 145°C and a large exothermic peak at 273°C. The physical interpretation of the large exothermic heat flow near the melting region in the NR curve is a subject of current controversy [17, 20]. Among these different molecular weights, heat flow area, ΔH^{NR}, follows the rank ordering: F-200 > F-214 > F-300. Thermal properties and initial degree of crystallinity of the cold ciystallized samples are listed in Table 2.

The crystal mass fractions of the constituent phases were also determined from WAXS of well-crystallized samples and are listed in Table 3. All the PPS samples have a mass fraction crystallinity, χ_c, of 0.25–0.26 from WAXS, very close to that determined from MDSC.

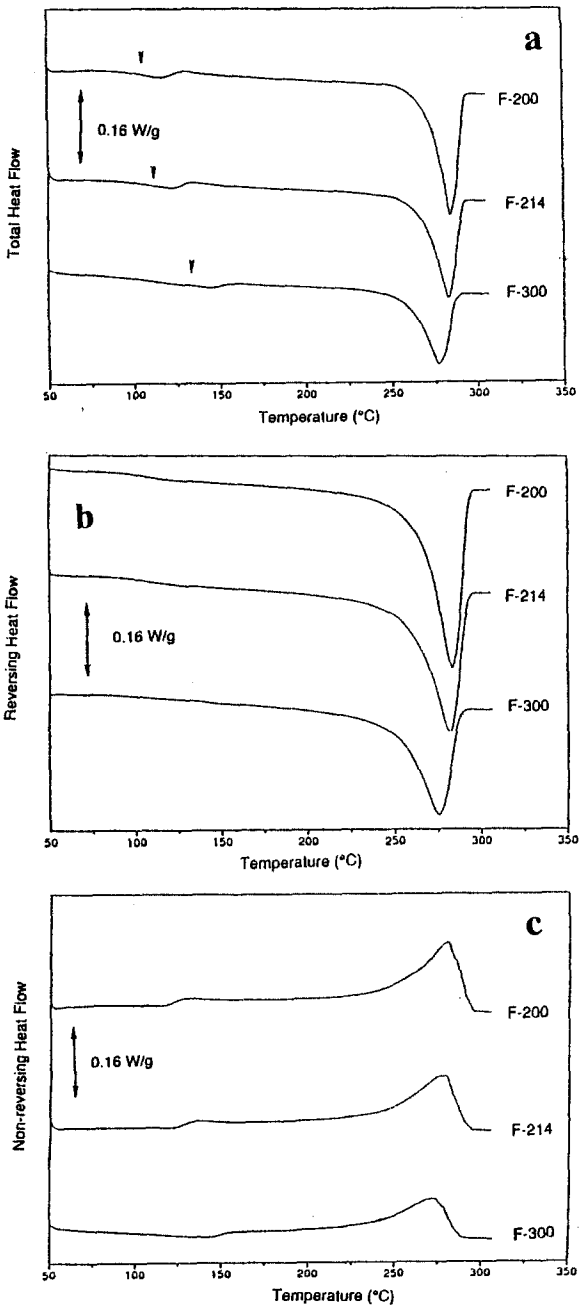

Fig. 3 MDSC heat flow curves for F-200, F-214, and F-300 Fortron™ PPS scanned at a rate of 5°C min^{-1}, with oscillation amplitude of 0.796°C and period of 60 s. a) total heat flow; b) reversing heat flow; and c) non-reversing heat flow *vs.* temperature

Table 2 Glass transition temperature, heat of fusion, ΔH, determined from MDSC* total, T, reversing, R, and non-reversing, NR, heat flow curves, and weight fraction crystallinity

Fortron PPS[a]	T_g/°C	ΔH^T/J g^{-1} (±0.3)	ΔH^R/J g^{-1} (±0.3)	ΔH^{NR}/J g^{-1} (±0.6)	χ_c^b
F-200	101	28.7	115.6	-86.8	0.25[6]
F-214	103	28.6	103.0	-74.5	0.25[5]
F-300	102	28.5	82.1	-53.4	0.25[4]

* Scanned at a rate of 5°C min^{-1}

[a] Crystallized at a temperature giving a half time of 200 s

[b] Determined from the area under the total heat flow curve; last digit is not significant but is shown to indicate the variation.

Analysis of the heat capacity step at the glass transition was used to determine χ_a, the amount of liquid-like amorphous phase contributing to the heat capacity step at T_g, $C_p(T)$, according to the following expression [2, 5, 6]:

$$\chi_a = \frac{C_p^{sc}(T)}{C_p^{a}(T)}\Bigg|_{T=T_g}$$

where the superscripts sc and a refer to the semicrystalline sample, and the completely amorphous sample, respectively. The fraction of amorphous phase constrained by the crystals at this scan rate (and not contributing to the observed heat capacity increment), χ_{ra}, was then found from:

$$\chi_{ra} = 1 - \chi_c - \chi_a$$

These results are listed in Table 3 for two different rates, a regular DSC rate of 20°C min^{-1}, and an MDSC rate of 5°C min^{-1}. For PPS crystallized with the same $t_{1/2}$, the higher molecular weight sample contains a larger χ_a. This indicates that a larger amount of liquid-like amorphous phase contributes to the glass transition heat capacity increment in the higher M_W sample.

The data indicate that there exists a large fraction of constrained amorphous chains inside the cold crystallized PPS. For different molecular weight samples with the same crystallization rate, the lower molecular weight sample exhibits a higher level of constraint. Current results on Fortron PPS agree well with our previous study on Ryton (Phillips Petroleum) PPS [5]. It suggests that crystals cause a very highly constrained amorphous phase interlayer, when T_c gets close to T_g. Also, a reduction in the scan rate causes more amorphous phase to be relaxed at T_g.

Conclusions

The effect of molecular weight on the cold crystallization behavior of Fortron™ PPS has been investigated using MDSC. Different molecular weights have about the

Table 3 Scan rate, mass fractions of crystal, χ_c, liquid-like amorphous, χ_a, and rigid amorphous phases, χ_{ra}, in cold crystallized Fortron PPS

Fortron PPS	Scan rate[a]/ °C min^{-1}	χ_c (±0.2)	χ_a (±0.2)[d]	χ_{rap} (±0.4)[d]
F-200	20	.26[b]	.20	.45
F-214	20	.25[b]	.24	.51
F-300	20	.26[b]	.29	.45
F-200	5	.25[c]	.31	.44
F-214	5	.25[c]	.35[5]	.39[5]
F-300	5	.25[c]	.41	.34

[a] 20°C min^{-1} regular DSC; 5°C min^{-1} MDSC
[b] Determined from WAXS
[c] Determined from ΔH^T, data listed in Table 2
[d] Third digit is not significant, but is shown to indicate the variation.

same crystallinity, whether measured from endotherm area or X-ray scattering. However, amounts of liquid-like and constrained amorphous phases differ among the different molecular weights. For samples crystallized with the same $t_{1/2}$, there is less mobile amorphous phase in the lower molecular weight material, which leaves it with a greater amount of constrained amorphous phase. These results suggest that there may be more taut-tie molecules between crystals of low molecular weight PPS, leading to greater constraints on amorphous phase mobility.

* * *

This research is supported by the U. S. Army Research Office through contract DAAH04-96-1-0009. The authors thank Hoechst Celanese for providing different molecular weight Fortron™ samples and Dr. George Collins for providing sample information. The authors acknowledge the assistance of Elizabeth Oyebode and Leonardo Grimaldi with sample preparation and MDSC work.

References

1 D. J. Brady, J. Appl. Polym. Sci., 20 (1976) 2541.
2 S. Z. D. Cheng, Z. Q. Wu and B. Wunderlich, Macromol., 20 (1987) 2802.
3 P. Cebe, Polymers and Polymer Composites, 3 (1995) 239.
4 J. S. Chung and P. Cebe, J. Polym. Sci., Polym. Phys. Ed., 30 (1992) 163.
5 P. P. Huo and P. Cebe, Colloid Polym. Sci., 270 (1992) 840.
6 P. Huo and P. Cebe, J. Polym. Sci., Polym. Phys. Ed., 30 (1992) 239.
7 L. C. Lopez and G. L. Wilkes, Polymer, 29 (1988) 106.
8 L. C. Lopez, G. L. Wilkes and J. F. Geibel, Polymer, 30 (1989) 147.
9 A. J. Lovinger, D. D. Davis and F. J. Padden, Polymer, 26 (1985) 1595.
10 J. D. Menczel and G. L. Collins, Polym. Eng. Sci., 32 (1992) 1264.
11 G. L. Collins and J. D. Menczel, Polym. Eng. Sci., 32 (1992) 1270.
12 D. R. Budgell and M. Day, Polym. Eng. Sci., 31 (7) (1991) 1271.

13 B. Hsiao, I. Chang and B. Sauer, Proc. 49th SPE ANTEC, XXXVII (1991) 2084.
14 S. X. Lu, P. Cebe and M. Capel, Macromolecules, in review, (1996).
15 M. Reading, B. K. Hahn and B. S. Crowe, US Patent 5,346,306 (1994).
16 M. Reading, Trends Polym. Sci., 8 (1) (1994) 248.
17 TA Instruments, Inc. MDSC Product Literature, (1995).
18 B. Wunderlich, Y. Jin and A. Boller, Thermochim. Acta, 238 (1993) 277.
19 A. Boller, Y. Jin and B. Wunderlich, J. Thermal Anal., 42 (1994) 307.
20 W. Sichina, Proc. 24th NATAS Conference, San Francisco, 1995, p. 123.